JOURNAL OF GEOPHYSICAL RESEARCH, VOL. 99, NO. E12, PAGES 26,015–26,028, DECEMBER 25, 1994

Structural history of Maxwell Montes, Venus: Implications for Venusian mountain belt formation

Myra Keep and Vicki L. Hansen

Department of Geological Sciences, Southern Methodist University, Dallas, Texas

Abstract. Models for Venusian mountain belt formation are important for understanding planetary geodynamic mechanisms. A range of data sets at various scales must be considered in geodynamic modelling. Long wavelength data, such as gravity and geoid to topography ratios, need constraints from smaller-scale observations of the surface. Pre-Magellan images of the Venusian surface were not of high enough resolution to observe details of surface deformation. High-resolution Magellan images of Maxwell Montes and the other deformation belts allow us to determine the nature of surface deformation. With these images we can begin to understand the constraints that surface deformation places on planetary dynamic models. Maxwell Montes and three other deformation belts (Akna, Freyja, and Danu montes) surround the highland plateau Lakshmi Planum in Venus' northern hemisphere. Maxwell, the highest of these belts, stands 11 km above mean planetary radius. We present a detailed structural and kinematic study of Maxwell Montes. Key observations include (1) dominant structural fabrics are broadly distributed and show little change in spacing relative to elevation changes of several kilometers; (2) the spacing, wavelength and inferred amplitude of mapped structures are small; (3) interpreted extensional structures occur only in areas of steep slope, with no extension at the highest topographic levels; and (4) deformation terminates abruptly at the base of steep slopes. One implication of these observations is that topography is independent of thin-skinned, broadly distributed, Maxwell deformation. Maxwell is apparently stable, with no observed extensional collapse. We propose a "deformation-from-below" model for Maxwell, in which the crust deforms passively over structurally imbricated and thickened lower crust. This model may have implications for the other deformation belts.

Introduction

Maxwell Montes is one of four deformation belts (Akna, Freyja, Danu and Maxwell Montes) that surround the highland plateau Lakshmi Planum in Venus' northern hemisphere (Figure 1). Lakshmi Planum rises 4 km above mean planetary radius (MPR) with the fringing deformation belts at elevations of ~5 km (Danu), 6 km (Akna), 7 km (Freyja), and 11 km (Maxwell) above MPR. Outboard of Lakshmi Planum, all the deformed belts are adjoined by areas of intensely wrinkled, complexly deformed crust known as tesserae, which lie at an average elevation of 5 km. Together, Lakshmi Planum, the deformation belts and the tesserae define a continent-sized region referred to as Ishtar Terra.

Maxwell Montes lies at the eastern edge of Lakshmi Planum. It is the highest and steepest feature on Venus, towering 4 km above Freyja Montes, the next highest of the Venusian deformation belts. It occupies an area ~850 km long by 700 km wide, and the adjacent tessera, western Fortuna Tessera, covers an area greater than 1.5 million km^2. Maxwell is characterized by dominant, northwest-trending, radar-bright lineaments, and an impact crater, Cleopatra (the highest crater on Venus), that lies on the eastern slope. Ejecta from Cleopatra covers most of central Maxwell, obscuring structures beneath; lava from a small rille from the crater floods ~64,000 km^2 of eastern Maxwell and western Fortuna Tessera. The steep northern, western and southern slopes of the mountain range vary in slope from 2° over ~300 km (north and south), to 30° over several tens of kilometers (west) [*Smrekar and Solomon*, 1992]. Deformation terminates abruptly at the base of these steep, deformed slopes. The eastern slope of Maxwell grades into western Fortuna Tessera.

Maxwell Montes is enigmatic because of its vast elevation. Any mechanism for the support of Maxwell must also apply to Ishtar Terra as a whole, and thus have significant impact on planetary geodynamic models. Most workers favor dynamic support for Ishtar Terra [e.g., *Pronin*, 1986; *Basilevsky*, 1986; *Kiefer and Hager*, 1989; *Bindschadler et al.*, 1990; *Grimm and Phillips*, 1990, 1991; *Bindschadler and Parmentier*, 1990]. *Grimm and Phillips* [1991] provide a discussion of the geophysical merits of isostatic versus dynamic models.

Current dynamic-support models for Ishtar Terra suggest that it is the site of either local mantle upwelling [*Pronin*, 1986; *Basilevsky*, 1986; *Grimm and Phillips*, 1990, 1991], or mantle downwelling [*Bindschadler et al.*, 1990, 1992; *Bindschadler and Parmentier*, 1990; *Lenardic et al.*, 1991]. In order to evaluate variations in crustal density, topography and gravity, both models use scales greater than those observed for the individual deformation belts of Ishtar Terra. As a result, none of these models are capable of predicting the nature of structures, orientations or kinematics within the Ishtar deformed belts, although on a broad scale mantle-upwelling and -downwelling mechanisms provide a means of local crust/mantle thickening around Ishtar Terra.

Paper number 94JE02636.
0148-0227/95/94JE-02636$05.00

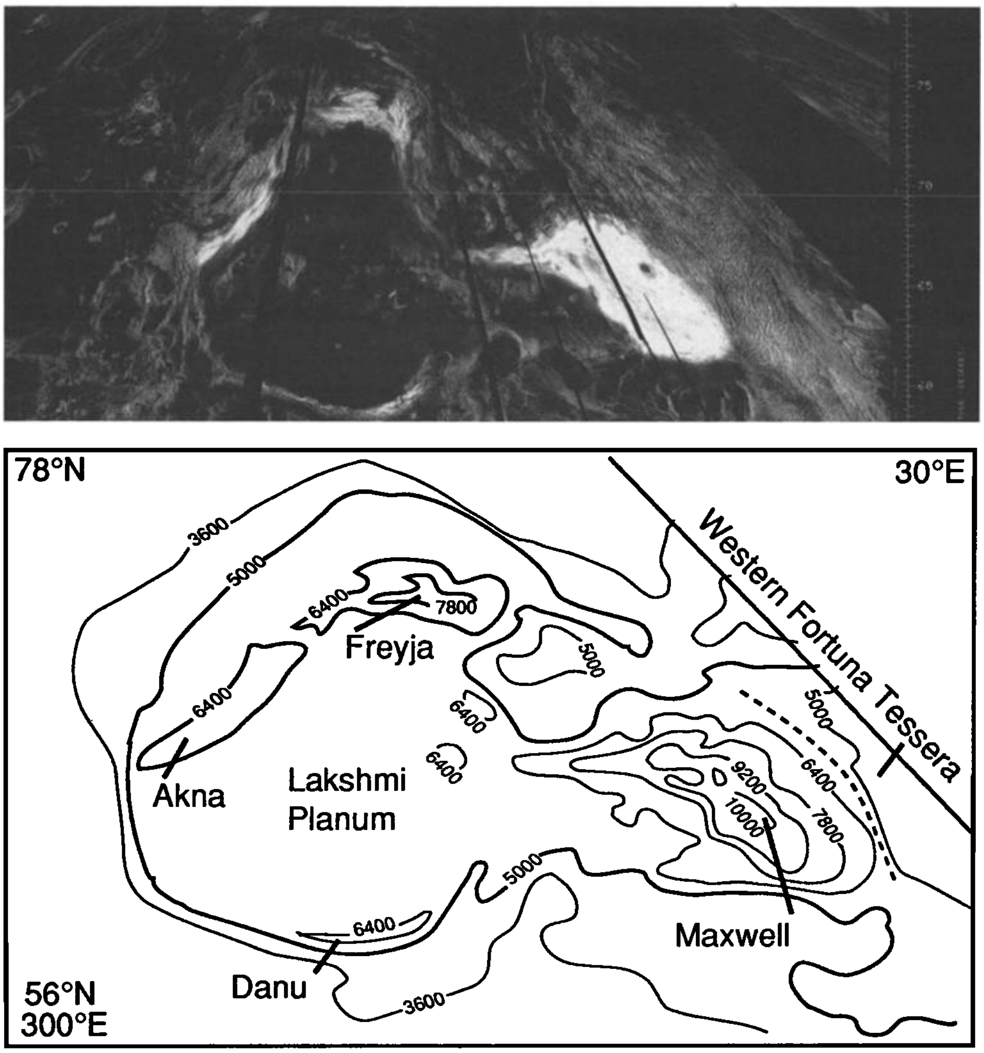

Figure 1. (a) Portion of Magellan C2-MIDRP.60N333;2 showing Ishtar Terra, including Akna, Freyja, Danu, and Maxwell Montes, and adjacent tesserae. Black areas are missing data. (b) Topographic contours for area represented in Figure 1a. Contours are in meters. Dashed line is eastern sinuous boundary lineament.

The character, wavelength, and spatial distribution of structures on Maxwell provides constraints for the surface and crustal deformation of individual Ishtar mountain belts. Geophysical data provide global constraints on lithosphere- and mantle-scale structures. The constraints from each of these data sets together provide insights into mechanisms of mountain belt formation. Current models for the structural evolution of Maxwell [*Vorder Bruegge and Head*, 1989; *Vorder Bruegge et al.*, 1990] did not have the benefit of high-resolution Magellan images, and some structures predicted by these models are not seen in Magellan data. This paper presents a structural analysis of Maxwell Montes. We use our observations to propose a mechanism for the deformation and support of Maxwell, in which the upper crust deforms passively over a structurally imbricated and thickened lower crust layer that supports the short-wavelength (500 km) mountain-belt-scale topography [e.g. *Phillips and Hansen*, 1994]. The favored model explains the observed deformation features of Maxwell Montes, and it may have implications for other Ishtar deformation belts.

Physiographic Divisions

Maxwell Montes comprises five physiographic provinces: the northwest arm, the eastern and western ridges, the area associated with the impact crater Cleopatra, and the southern slope (Figure 2). These provinces are discussed in turn below.

The northwest arm comprises a triangular-shaped region that juts westward from the main body of the mountain belt. It is separated from the rest of Maxwell by a sinuous lineament that trends southwest from 69°N, 4°E to 66.5°N, 359°E , and then trends south to 65°N, 0°E, where it marks the western boundary of Maxwell, extending to 61.5°N, 2°E (Figure 2). This lineament is herein referred to as the 0°E lineament. Most of the northwest arm is at lower elevation than the main body of Maxwell. The highest area of the arm (~10 km above MPR) is centered around 66.4°N, 357.5°E, and elevations decrease in all directions away from the 0°E lineament, to a low of ~5.5 km above MPR around 67.3°N, 353.5°E. The northern flank of the arm slopes 2° over ~300 km [*Smrekar and Solomon*, 1992].

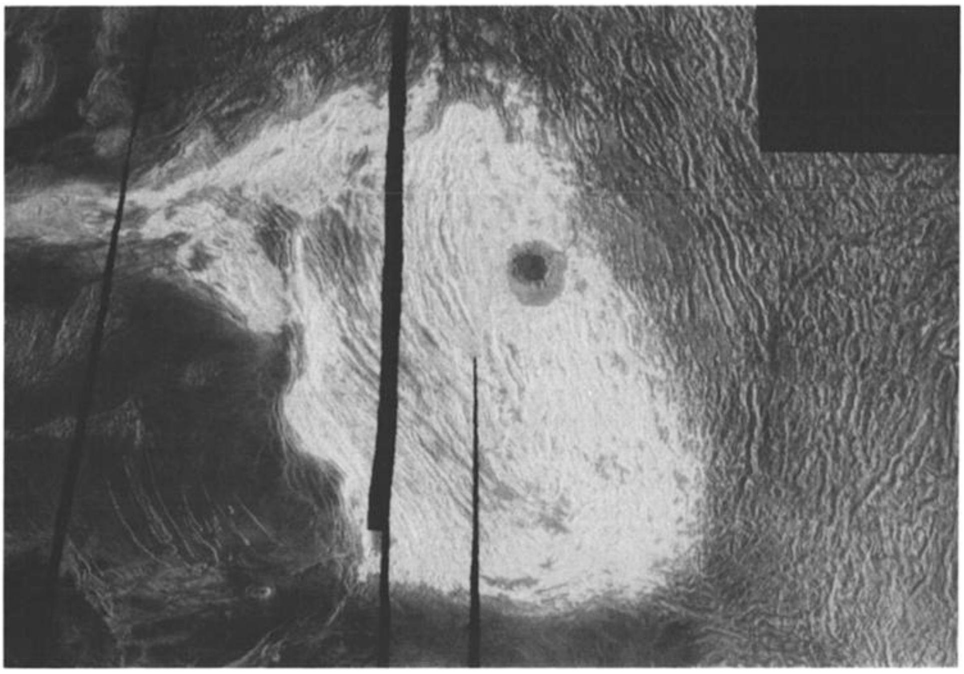

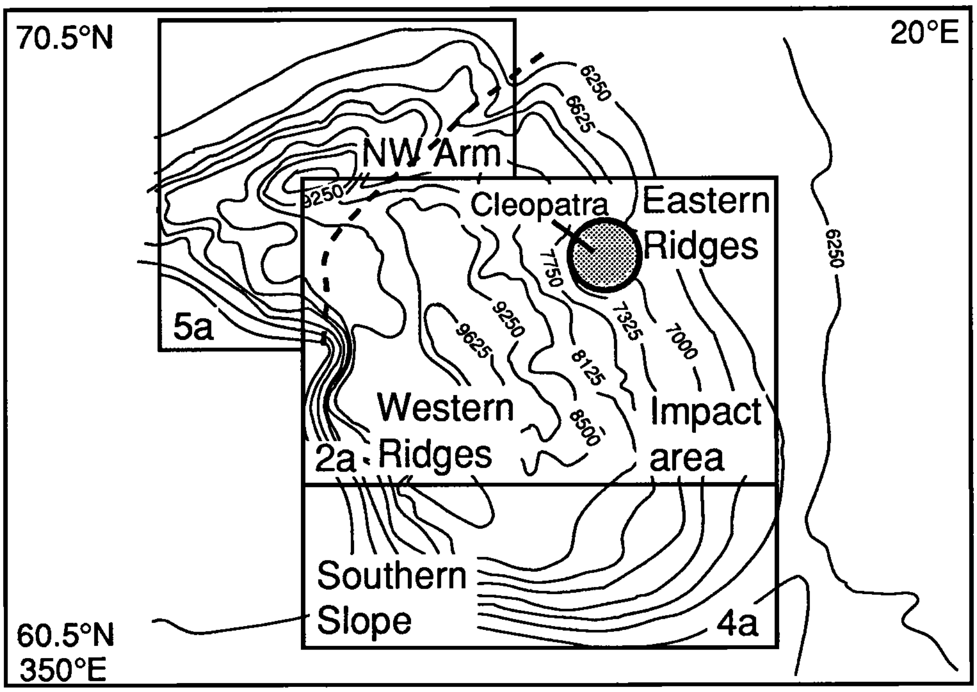

Figure 2. (a) Composite image of Maxwell Montes. Black stripes are missing data. Dark circle at center is the impact crater Cleopatra. The 0°E lineament is visible as offset of radar-dark material at left, just above center. (b) Topographic contours for Figure 2a showing the physiographic provinces described in the text, locations of Figures 2a, 4a and 5a, and the location of the 0°E lineament described in the text, shown as dashed line.

The eastern and western ridges, crater-modified area, and the southern slope are all part of the main body of Maxwell Montes. Transitions between these physiographic provinces are gradational; they are distinguished on elevation changes and extent of impact ejecta, both of which cause variations in radar-brightness. The northern boundary of the main body of Maxwell is the 0°E lineament. Steep elevation changes mark the western and southern boundaries between Maxwell and adjacent plains; the eastern boundary, a sinuous trough, extending from 62.5°N, 11° to 68°N 10°E, marks the beginning of an ~200 km transition between Maxwell and western Fortuna Tessera.

The eastern ridges encompass the radar-dark area east of Cleopatra, extending from 63° to 68°N, and 9° to 13°E. They occupy the topographically lowest part of Maxwell, ranging from 6.5 to 5.5 km above MPR over a distance of ~200 km, defining the shallowest slope of Maxwell. The western ridges are bound to the north by the 0°E lineament, and to the west by a steep slope between Maxwell Montes and the relatively undeformed Lakshmi Planum. To the east the western ridges grade into the crater-modified area. They occupy the highest region of Maxwell (average elevation >10 km), although the western boundary is steep, with a slope of 30° over several tens of kilometers. A radar-bright band of Cleopatra ejecta extending from 63° to 68°N, 4° to 8°E separates the eastern and western ridges. This band, hereafter referred to as the impact region, spans an elevation range of 6 to 9 km above MPR and somewhat obscures features beneath it. To the east and west, relatively abrupt changes in radar brightness define the boundaries of this region. The eastern and western ridges, and the impact region, grade south into a narrow, approximately east-trending band of radar-bright material that defines the southern slope. The slope in this region is 2° over ~300 km, and evidence of crustal deformation terminates abruptly at this transition.

Radar Image Interpretation

Magellan synthetic-aperture radar (SAR) images derive from echoes of electromagnetic energy pulses transmitted perpendicular to the line of flight of the Magellan spacecraft. Analysis of the intensity, time delay, and frequency shift of the echoes produces image resolution elements that are assigned a brightness level corresponding to the strength of the echo [*Ford et al.*, 1989]. The resultant images are surface representations of echo strength (i.e., brightness). Radar brightness is controlled primarily by surface slope and surface roughness. Surfaces oriented approximately perpendicular to the incident beam reflect the greatest amount of radar energy, producing a strongly radar-bright area. Surface slopes oriented away from the radar produce weaker, thus darker, areas on the SAR images. This effect emphasizes topography and varies with the change in look angle of the radar beam at different latitudes [*Ford et al.*, 1989; *Farr*, 1993]. Surface roughness affects image brightness in the following way: given uniform slope, smooth surfaces (e.g., flood-type lava flows) reflect most of the radar energy away from the receiver and are therefore dark on radar images, whereas rough surfaces (e.g., deformed areas) cause scattering of radar echoes in all directions, resulting in radar-bright areas [*Ford et al.*, 1989; *Farr*, 1993]. More detailed discussions on Magellan SAR imaging and the effects of surface slope and roughness can be found in *Ford et al.* [1989, 1993], *Saunders and Pettengill* [1991], *Pettengill et al.* [1991], *Saunders et al.* [1992], *Ford and Pettengill* [1992], *Tyler et al.* [1992], and references therein.

Surface radar-brightness is therefore a useful tool for structural mapping on Venus. Changes in radar-brightness, and the texture of radar-bright areas, allow interpretation of relative topography and/or surface roughness (i.e., deformation). Within the overall radar-bright or -dark framework, physiographic and geologic features, generally manifested as lineaments, may be discerned on the basis of shape (straightness or sinuosity), spacing, length, nature of changes between radar-bright and -dark areas (either gradual or abrupt), and whether structures are paired or single [*Stofan et al.*, 1993]. We emphasize here that physiographic features discernible on SAR imagery must be distinguished from a geologic interpretation of them.

Single lineaments have several forms. In Ishtar Terra, some single lineaments are long, slightly anastomotic, radar-bright along one side, and have gradual transitions in brightness across them. These features are generally interpreted to be physiographic ridges, with bright radar-facing slopes becoming progressively more radar-dark where they dip away from the radar [e.g., *Ford et al.*, 1989, 1993]. This effect is enhanced if the ridges are oriented perpendicular to the radar beam, and becomes progressively weaker with smaller angles between ridge orientation and radar direction. Ridges are commonly interpreted as folds [e.g., *Campbell et al.*, 1983; *Crumpler et al.*, 1986; *Head*, 1990; *Solomon et al.*, 1991, 1992; *Kaula et al.* 1992; *Stofan et al.*, 1993], and thus of contractional origin. Radar-dark areas between bright ridge crests should be topographically lower than the crests (i.e., valleys), a phenomenon observed locally by the apparent filling of these topographic lows by radar-smooth material, interpreted as flood-type lava flows. *Stofan et al.* [1993] interpreted the gradual tonal transition across ridges as paired light and dark lineaments, whereas we define them as singular bright lineaments with gradual tonal changes; either interpretation is correct.

Other single lineaments are thin, sharp, and straight, and they show either uniform radar reflectivity or have sharp tonal contrasts at the ridge scarp. These sharp lineaments often end against other lineaments, or other lineaments end against them, resulting in juxtaposition of contrasting radar-bright areas. On Earth, such features are commonly interpreted as fractures [e.g., *Ford et al.*, 1989], and we follow this interpretation for Venus [*Stofan et al.*, 1993].

Paired lineaments are commonly straight, parallel, and separated by radar-smooth material. One slope of the pair is radar-bright toward the center, whereas the other is radar-dark, indicating oppositely dipping slopes toward the center of the lineament pair. These features are typically interpreted to be graben, with the paired lineaments representing bounding normal faults and the radar smooth material representing graben floors [*Smrekar and Solomon*, 1992; *Stofan et al.*, 1993]. Radar smooth graben floors may preserve radar brightness contrasts or may be uniformly radar bright. Generally, the transition across one lineament to the interpreted graben floor is sharp, in contrast to the gradual transition in radar brightness across ridges. These graben are interpreted as evidence of local crustal extension [e.g., *Basilevsky et al.*, 1986; *Bindschadler and Head*, 1991; *Solomon et al.*, 1991; *Smrekar and Solomon*, 1992].

Although limited to two-dimensional images of the Venusian surface, we may determine the relative timing and depth of extension fractures from their spacing and orientation with respect to topography. Terrestrial fracture studies indicate that terminated fractures are younger than older, through-going fracture sets, because the older fractures act as a free surface blocking propagation of younger, terminated fractures [e.g., *Engelder and Geiser*, 1980; *Pollard and Aydin*, 1988]. Fracture fill is important, and if an older, through-going fracture is filled, it no longer acts as a free surface, so younger fractures may propagate across it. Also, if a younger fracture initiates at greater depth than an older fracture, it may propagate beneath and around the older fracture. Fracture spacing is related to the depth of a fracture set; closely spaced or penetrative fractures indicate shallow depth, and more broadly spaced fractures indicate greater depths [e.g., *Engelder* *and Geiser*, 1980; *Pollard and Aydin*, 1988]. The relative dip of structures may be inferred from their interaction with topography. Steeply-dipping structures cut across topography with linear traces, whereas the trace of shallowly-dipping structures follows topography.

For Magellan data, some of the above relationships are further complicated. With side-looking radar there is an ambiguity in range introduced by elevation changes [*Ford et al.*, 1989], such that a vertical fracture with a straight strike will appear to wander laterally over varying topography, whereas a fault that dips shallowly away from the spacecraft at the complement of the look angle (look angle is measured from vertical; dip is measured from horizontal) will appear straight. Because the radar look angle for Maxwell is small (~25°), structures that dip steeply away from the look angle will appear straight, and will not wander laterally as predicted for structures affected by range ambiguities. We therefore employ the terrestrial relative timing and depth interpretations discussed above in our analysis.

Another geometric artifact that must be considered for SAR image interpretation is layover, or extreme foreshortening, which occurs at low incidence angles where topographic peaks are closer to the spacecraft than the base of the topographic element. In the resultant image, the mountain slope will be displayed in reverse relative to the illumination vector [*Ford et al.*, 1989; *Farr*, 1993]. Layover effects are enhanced by small look angles and steep slopes, both of which apply for Maxwell. In terms of structural analysis, one of the main effects of layover is that ridge asymmetry, and hence fold symmetry, cannot be uniquely determined [*Farr*, 1993; *Stofan et al.*, 1993]. In our discussion, we use spacing between ridge crests, rather than structural asymmetry, to infer structural history, without introducing problems caused by layover effects.

The spatial distribution of structures is important in determining strain history. During a single deformation episode, different crustal strains may be recorded at different locations. In our analysis, we identify families of lineaments around Maxwell Montes, interpret their structural nature, infer timing and depth relations between them, and use their spatial distribution to interpret strain history. Our structural analysis of Maxwell Montes uses Magellan SAR images, both full-resolution mosaicked image data records (F-MIDR's), and compressed-once data records (C-MIDR's) (areas of 5° x 5° and 15° x 15°, respectively), and individual framelets of each (56 framelets/MIDR). To minimize brightness bias, Magellan collected data with both right- and left-oriented radar look directions. Where available, we used both right- and left-looking images. We analyzed images both in hard copy and as digital images (CD-ROM) on a Sun Sparc 10 workstation.

Structural Styles

Structurally, the eastern and western ridges, southern slope, and the impact region comprise a single structural province defined by lineaments of similar character and orientation. Structures are best preserved on the western ridges and southern slope, regions that escaped impact and lava flooding, but they are also observed throughout the eastern ridges and impact region. The structural grain of this composite province trends northwest to north-northwest, parallel to topographic contours. The northwest arm of Maxwell Montes, separated from the main body by the 0°E lineament described above, preserves a similar structural fabric, but also displays structures not present in central Maxwell. Trends unique to the arm define a structural grain perpendicular to that of central Maxwell, but parallel to topography on the northwest arm. The change in orientation of structural grain and topography commences at the 0°E lineament. The 0°E lineament therefore marks a change in structural style and a break in topography. We interpret the 0°E lineament to be a fundamental structural discontinuity between central Maxwell and the northwest arm. The two provinces are described separately below.

Eastern and Western Ridges, Impact Region, and Southern Slope

We define four suites of structures on the main body of Maxwell Montes: (1) dominant northwest-trending ridges; (2) penetrative north-trending lineaments; (3) northwest-trending grabens, confined to the southern slope; and (4) northeast-trending grabens, located on the southern slope.

Northwest-trending ridges, characterized by narrow, west-facing, radar-bright slopes and broader, east-facing, comparatively radar-dark slopes, dominate the structural fabric of the area extending from the northwest arm to the southern slope (~700 km) (Figure 3). Facing directions of radar-bright and -dark areas do not necessarily imply structural asymmetry due to layover effects [*Farr*, 1993; *Stofan et al.*, 1993]. Ridges vary in length from 150 to 500 km and are relatively straight, although they do curve along their length. We interpret ridges as folds, due to the broad tonal transition from radar-bright to -dark across the ridge [*Stofan et al.*, 1993]. Three transects, oriented perpendicular to the trend of these ridges (Figure 3), illustrate the variation in ridge spacing, measured between the brightest part (crest) of each lineament, with distance and topography (Figure 4). Each transect crosses both the impact region and flooded areas where ridges are somewhat obscured; ridge spacing in these areas therefore represents a maximum. Ridge spacing in unmodified areas is relatively uniform, varying from ~6 to 10 km over distances of 800 km and elevation changes of >6 km. Where ridge spacing does increase it does so independent of changes in topography (Figure 4). These northwest-trending ridges continue 200 km into western Fortuna Tessera, where they gradually become indistinguishable from tessera deformation.

Radar-bright, wispy, north-trending lineaments comprise the second set of structures (e.g., between 3°E and 5°E, 64°N) (Figure 3). These lineaments are closely spaced, defining a penetrative fabric observed everywhere on central Maxwell except the southern slope. Interactions with the spaced ridges cause variations in strike direction and length of the penetrative lineaments; they strike generally north, except in proximity to a spaced ridge, where the strike changes and parallels the ridge. The length and continuity of the penetrative lineaments is therefore difficult to ascertain. The close spacing of these lineaments indicates shallow penetration depths. We interpret these lineaments as fold belts, possibly related to thrusts (fault-bend folds), due to their variations in strike; however, they may represent original extensional fractures, later contracted during crustal shortening (see Summary of Structural Styles below).

On the southern slope of Maxwell Montes, spacing of the dominant ridges increases as ridge orientation splays to the east-southeast. Valleys become prominent between the spaced ridges, and along the valley traces, straight, parallel, paired lineaments interpreted as grabens are observed [*Smrekar and

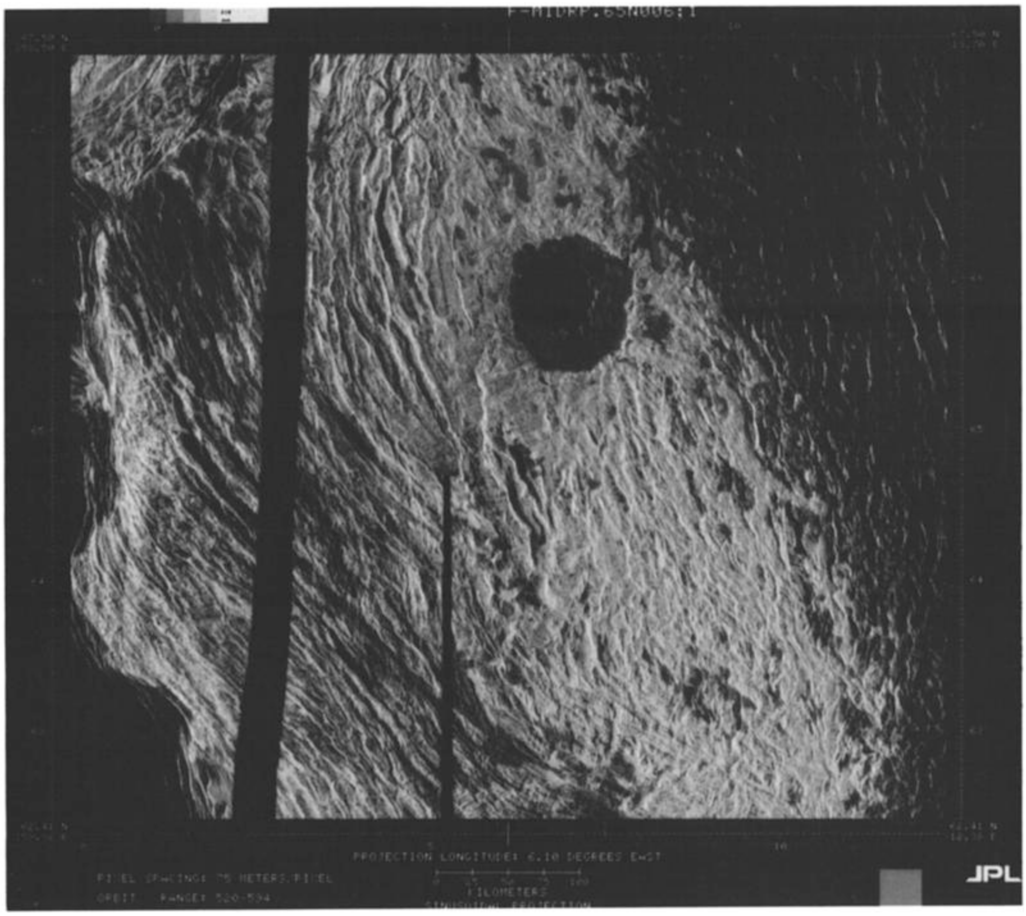

Figure 3a. Magellan F-MIDRP.65N006;1 showing detail of the main part of Maxwell Montes. Dark circular area is Cleopatra. Black stripes represent areas of missing data. Arrow is screen cursor.

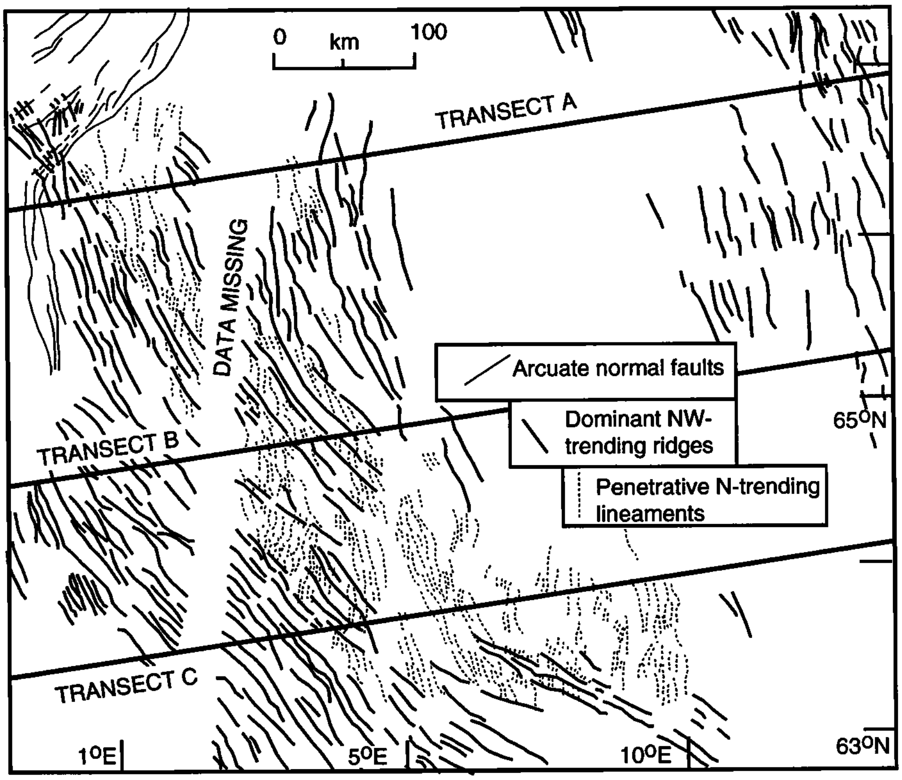

Figure 3b. Geologic intepretation of Figure 3a showing structural features, image latitudes and longitudes, and the location of transects in Figure 4 .

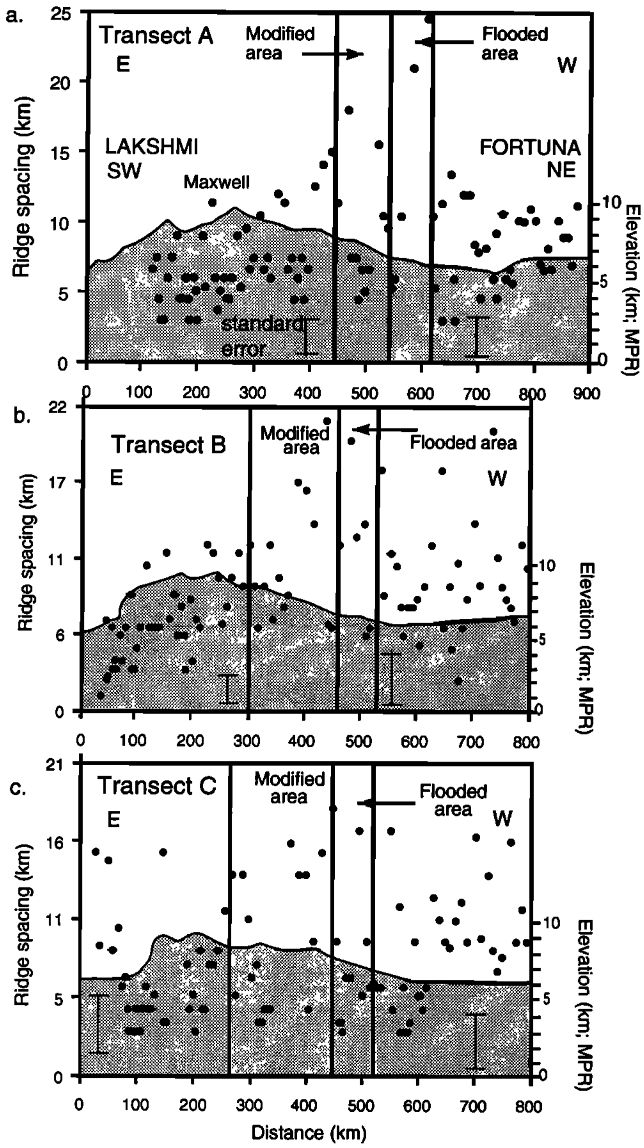

Figure 4. Topographic profiles of transects A, B, and C, showing ridge spacing across Maxwell Montes. Dots represent ridge spacings measured between ridge crests. Plots are divided into four sections: eastern unmodified section (E), western unmodified section (W), and flooded and modified sections. Error bars of standard error are given for the eastern and western areas. Topography has 35 X vertical exaggeration.

Solomon, 1992] (Figure 5). The grabens average 60 km in length, 7 km in width, and at their closest they are spaced ~10 km apart. Graben floors, although generally smooth, preserve variations in radar-brightness, indicating that they are not filled with flood-type lava. We interpret steeply-dipping graben-bounding faults based on the straightness of the lineaments relative to topography. Graben orientations suggest northeast-southwest (slope-normal) extension [*Smrekar and Solomon*, 1992].

The fourth set of structures trends northeast and occurs predominantly on the southern slope, in areas of 2° regional slope (Figure 5). This set comprises a series of narrow, straight, paired, parallel-sided lineaments, with an average length of 20 km, interpreted to be grabens [*Smrekar and Solomon*, 1992]. Graben floors are generally smooth, but, like the northwest-trending grabens, they preserve variations in radar brightness, indicating that they are not lava filled. Graben orientation is consistent with northwest-southeast (slope-parallel) extension.

Timing relations between the four structural suites described above are inferred on the basis of cross-cutting relations and spatial location. The penetrative lineaments are the only structures that display variation in strike, from ridge-parallel in proximity to a spaced ridge, to generally north-trending elsewhere. The result is that the penetrative lineaments are modified to a sigmoidal form due to interaction with northwest-trending ridges and grabens. The sigmoidal nature of the interference is similar to S-C shear geometries in terrestrial shear zones [*Berthé et al.*, 1979]. However, in S-C structures, the S (penetrative) and C (non-penetrative) shear planes form synchronously and require specific angular relationships (0-45°). Although the penetrative and spaced lineaments are commonly <45° apart (e.g., central Maxwell), in southern Maxwell they are perpendicular to one another (Figure 3b). These angular relations are not compatible with S-C geometry, but rather with crenulation cleavage development [*Ramsay and Huber*, 1983], in which one planar fabric overprints another. The penetrative lineaments and the spaced ridges are therefore not synchronous; the spaced ridges and grabens postdate formation of the penetrative lineaments.

The spaced ridges and northwest-trending grabens parallel one another, with the grabens generally located in the valleys between the spaced ridges. The grabens are prominent to the southeast and are spatially limited to the southern slope; the ridges are prominent elsewhere to the northwest on Maxwell. Both sets of structures crosscut the penetrative lineaments but are themselves cut by northeast-trending grabens on the southern slope. We therefore infer the northwest-trending grabens and the spaced ridges to be essentially coeval, forming in different places at the same time. Geologically it is easier to envision preservation of early-formed ridges, with later graben development, than the preservation of early-formed grabens during later contraction. We therefore interpret the grabens as being relatively younger than the northwest-trending ridges, although absolute timing relations cannot be discerned.

The northeast-trending grabens on the southern slope crosscut both the spaced ridges and the northwest-trending grabens. In places, the northeast-trending grabens also crosscut the penetrative lineaments, causing irregularly-shaped depressions that have the tips of the penetrative lineaments and parts of the ridges preserved as "islands" (e.g., 63°N, 6°E). We therefore interpret the northeast-trending grabens to be the youngest of the four structural suites.

Relative timing between structural suites is thus (1) penetrative lineaments,(2) spaced ridges,(3) northwest-trending grabens, and(4) northeast-trending grabens, although all four suites may be manifestations of progressive deformation. Both graben sets occur only in areas of steep topographic slope, suggesting that extension is related to the abrupt decrease in topography, with extension directions both parallel and perpendicular to slope.

Northwest Arm

The northwest arm, in addition to the four structural suites described above, contains three other sets of structures. Vestiges of the first-formed, penetrative lineament fabric are

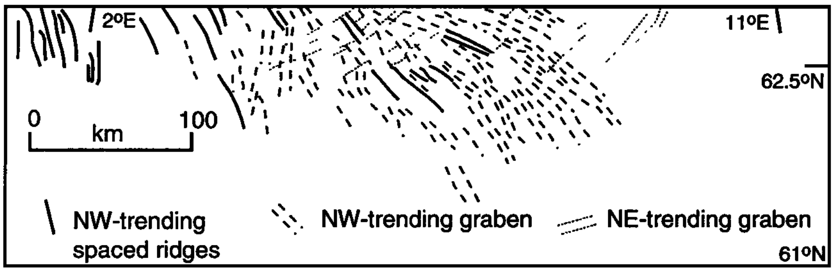

Figure 5. (a) Portion of F-MIDRP.60N005;1 showing southern slope of Maxwell. Black stripes represent missing data. (b) Generalized structure map of area in Figure 5a, showing interpreted structures and image boundaries.

restricted to a small area around 67°N, 0°E. The spaced ridges dominate the northwest arm, but are spatially separate from the penetrative lineaments, so the crenulation cleavage-type fabric is absent. Northwest-tending grabens between the spaced ridges are prominent in areas of steep topography on the northern slope, but they do not fan out as they do on the southern slope (Figure 6). They extend to the northern terminus of the mountain range, recording local northeast-southwest extension (i.e., normal to slope). Northeast-trending grabens also occur in areas of steep slope, but they are closely spaced, forming a penetrative fabric that extends from ~67°N, 355°E, to 68°N, 357°E. These grabens record northwest-southeast (slope-parallel) extension (Figure 6). Relative depths and dips of these structures are inferred to mimic those in central Maxwell. However, cross cutting relations between the northwest-trending grabens, and the here penetrative northeast-

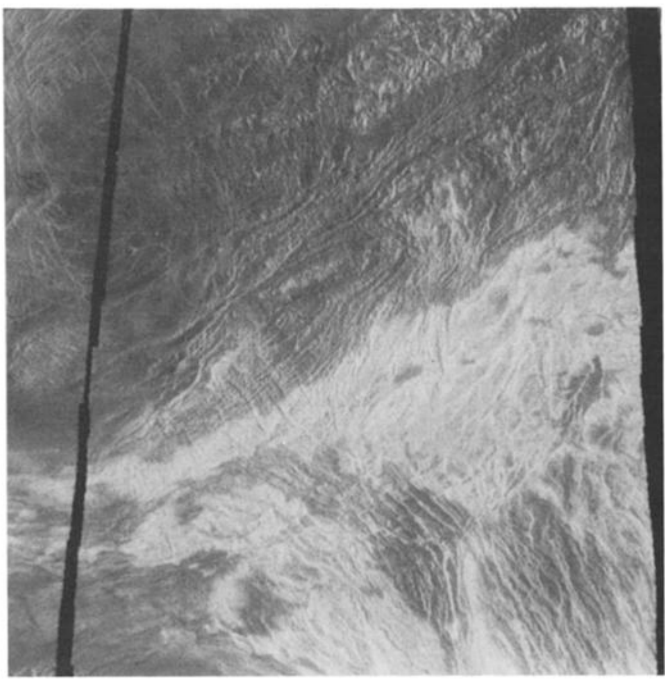

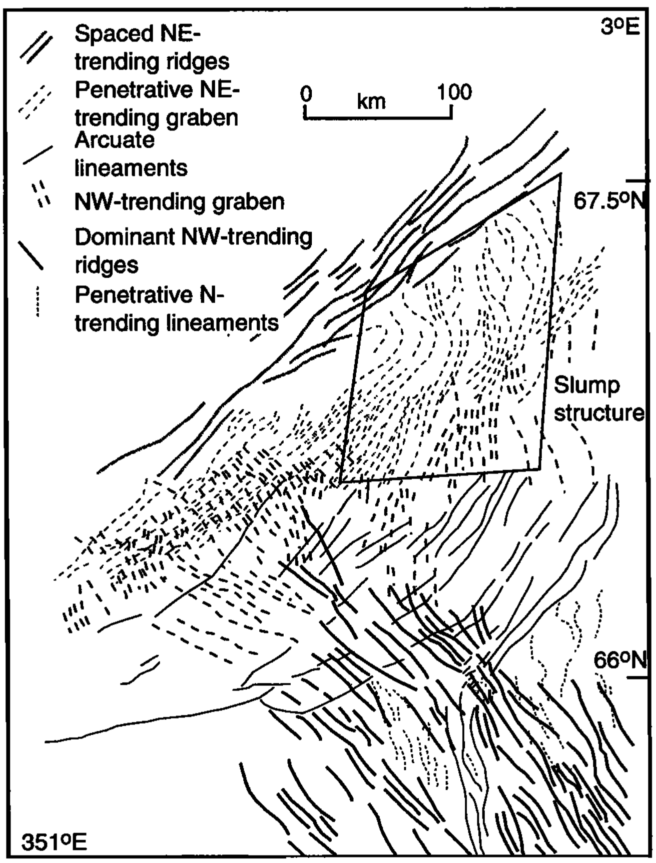

Figure 6. (a) Composite image of northwest arm and slump structure of Maxwell Montes. Black stripes are missing data. (b) Generalized structure map of area in Figure 6a, indicating image boundaries and the location of the slump structure. Note that the strike of penetrative northeast-trending graben is modified in the vicinity of the slump.

trending grabens are more complex (see discussion of timing relationships below).

A fifth set of structures, unique to the northwest arm, comprises arcuate lineaments that trend northeast in the northern part of the arm and west-southwest in the west part of the arm. The arcuate lineaments are long (>200 km), thin, relatively continuous, sporadically spaced (30 to 55 km), sharp, and generally radar-bright. Several of the lineaments bifurcate (e.g., 66.4°N, 356°E), and many northwest-trending ridges terminate abruptly at the lineaments. We suggest that the lineaments mark sharp, concentric faults (Figure 6). Their continuity with respect to topography indicates relatively steep dips, and their broad spacings are indicative of relatively deep penetration. The shape and distribution of these structures are reminiscent of rotational normal faults in landslip or slump areas [*Varnes*, 1958], and would, in this case, indicate down-drop to the northwest, consistent with topography.

An irregularly shaped structure (the sixth set) lies at the northeastern-most extension of the arm, around 68.1°N, 0°E (Figure 6). This structure is bounded by northeast-trending ridge-graben pairs, the orientations of which are deflected to enclose a balloon-shaped area on the steep northern slope. The center of the structure is filled with deflected penetrative grabens that become randomly oriented downslope. The irregular shape of the structure, the deflection of grabens around the structure and the random orientation of lineaments at its center, lead us to suggest that the structure formed as result of slumping, possibly related to the steep topographic gradient and local extensional deformation. Similar interpretations for this structure have been suggested by *Kaula et al.* [1992].

A seventh set of structures bounds the slump structure to the northwest (Figure 6). This set comprises spaced, northeast-trending, continuous lineaments, that extend from ~ 67.5°N, 354°E, to 69.4°N, 1°E. The lineaments are radar-bright on their northwest sides, and they are separated by parallel, paired, continuous, radar-dark bands. We interpret these features to be ridges, separated by narrow grabens, respectively. The ridge spacing (~6 km) is greater than that of the penetrative, northeast-trending grabens. At 67.5°N, 355°E and 68.2°N, 0°E, the penetrative northeast-trending grabens are deflected by these spaced ridges, forming sigmoidal shapes that trend into parallelism with the spaced ridges as they intersect. The spaced northeast-trending ridges on the northern slope of Maxwell essentially bound the deformation, although traces of northwest-trending lineaments parallel to those on Maxwell grade into the plains around 69°N, 355°E.

Vestiges of the penetrative fabric, the spaced ridges and the northwest-trending grabens have similar spatial relations to those observed for analogous structures on central Maxwell. We therefore infer similar timing relations between them: (1) penetrative lineaments, (2) spaced ridges, (3) northwest-trending graben, and (4) northeast-trending grabens. Temporal relations between the two graben sets, and among other structural suites on the northwest arm, are more complex.

As discussed above for central Maxwell, northwest-trending grabens are inferred to be older and deeper than northeast-trending grabens that crosscut them, with both sets of structures confined to areas of steep topography. However, on the northwest arm, mutual cross-cutting relations exist between the graben sets. Most of the northwest-trending grabens disappear toward the northern terminus of Maxwell (inferring progressively shallower depths), and are crosscut by the penetrative northeast-trending grabens. However, several northwest-trending grabens are prominent, with inferred deep depths; these grabens crosscut the penetrative northeast-trending grabens. Cross-cutting relations are dependent, in part, on the depth of the structures involved: older structures, where deep and/or unfilled, may apparently truncate younger, shallow structures; conversely, young structures may propagate under or across older structures where the latter are shallow and/or filled. We therefore propose that the northwest-trending grabens are generally older and deeper than the northeast-trending grabens (as on central Maxwell), but that at the northern slope break, the younger northeast-trending grabens are locally deeper, resulting in mutual cross-cutting relations.

We interpret the slump structure to be younger than penetrative northeast-trending ridge-graben pairs that bound it, as the slump structure apparently deflects the latter. Similar apparent deflection of structures may occur if the slump was a rigid object around which the folds formed. However, by definition, a slump is not a rigid body, and we propose that it postdates the penetrative northeast-trending ridge-graben pairs. Similarly, we suggest that the spaced northeast-trending ridges that essentially bound Maxwell deformation are the youngest structures on the arm, as they physically bound the slump and locally modify the trend of the penetrative grabens.

The arcuate faults cut the northwest-trending grabens at the head of the slope, inferring that they are younger than the northwest-trending grabens, but are otherwise not temporally constrained. We interpret them to postdate the northwest-trending grabens, and to be related to downslope failure. They may have formed at any time before or during the development of the slump structure.

Summary of Structural Styles

Central Maxwell and the northwest arm share similar deformational histories up to the time of formation of the northeast-trending grabens (i.e., penetrative lineaments, spaced ridges, northwest-trending grabens, northeast-trending grabens). We briefly discuss formation of structures common to both central Maxwell and the northwest arm, and then those unique to the northwest arm.

The penetrative lineaments and the northwest-trending ridges are contractional structures, folds, possibly thrust-related, and thus are interpreted to have formed during overall crustal shortening. The two structural suites may be manifestations of a single, progressive, non-coaxial deformation episode, with the penetrative lineaments reflecting either an early phase of deformation, or an earlier, unrelated episode of crustal contraction. It is also possible that the penetrative lineaments represent original, early-formed, parallel lineations of *Banerdt and Sammis* [1992], formed as a result of lineation-normal extension, that were later contracted during crustal shortening, as they are found throughout Ishtar deformed belts [*Phillips and Hansen*, 1994; *Hansen and Phillips*, 1993]. Northeast-trending grabens on the southern slope parallel the direction of maximum shortening interpreted from the spaced ridges, and are thus compatible with a single strain regime. Northwest-trending grabens on the southern slope are not compatible with a single strain regime, as they parallel the spaced ridges. However, the spatial restriction of the northwest-trending ridges to the steep southern slope may indicate that their distribution is somewhat controlled by topographic gradient, and is thus related to the mechanism of mountain belt support. We therefore conclude that the main structures of both central Maxwell and the northwest arm (penetrative ridges, northwest-trending ridges, northwest-trending grabens, northeast-trending grabens) are compatible with deformation during regional crustal contraction, with late, local, northeast extension along the southern slope.

Almost all structures unique to the arm are interpreted as extensional features (oriented perpendicular to slope), and are associated with steep topographic slope. We suggest that the penetrative northeast-trending grabens, the arcuate lineaments, the slump structure and the spaced northeast-trending ridges bounding the slump are manifestations of downslope extension, perhaps related to gravity sliding [*Smrekar and Solomon*, 1992]. In support of this hypothesis, the spaced northeast-trending ridges (the sixth set of structures described from the arm) occur near the break in slope with the plains to the north. Similarly, the slump extends downslope, and is terminated by spaced northeast-trending ridges at the slope break. The arcuate lineaments (interpreted normal faults) occur further upslope. The dense distribution of structures at the slope base, with more widely spaced structures upslope, is consistent with formation due to slumping [e.g., *Varnes*, 1958, *Shreve*, 1968].

Central Maxwell and the northwest arm appear to have been deformed simultaneously for most of their respective deformation histories, as shown by several structural similarities: (1) the dominant structural fabrics parallel topographic contours, are broadly distributed, and show no change in spacing relative to elevation changes; (2) structures on Maxwell Montes have relatively short wavelengths and close spacing with respect to elevation; (3) grabens occur only in areas of steep slope (>2°); (4) no grabens occur in areas of highest topography; and (5) deformation terminates abruptly in areas of steep slope (with the exception of the more gentle transition to western Fortuna Tessera. Extensional structures related to gravity sliding occurred late in the deformation history of the northwest arm.

Discussion

Our observations of structural styles on Maxwell Montes have several implications. Broadly distributed deformation, over several hundred kilometers perpendicular to strike and elevation changes of several kilometers, suggests that deformation is independent of topography. Similarly, topography is independent of deformation (i.e., not structurally supported); assuming fold amplitudes of <2 km [*Hansen and Phillips*, 1993], deformation is modest, and not able to support the 12 km elevation of Maxwell. If the elevation of Maxwell derives from crustal thickening alone, then fold amplitudes of tens of kilometers are implied, which is difficult to envision given the regular ridge spacing of 6-12 km, and no apparent structural break parallel to ridge traces. Lack of extensional structures at the highest elevations of the belt suggest a lack of extensional collapse; therefore, Maxwell crust is apparently stable at elevations of 11 km. Tectonic models for the formation of Maxwell Montes must address these observations and implications.

Models for the tectonic evolution of venusian mountain belts fall into two groups, those addressing Ishtar Terra as a whole, and those specifically addressing Maxwell Montes. We give a brief overview of each of these groups, and then present a new model for the tectonic evolution of Maxwell Montes.

Tectonic Models for Ishtar Terra

Models for the formation of Ishtar Terra propose that Lakshmi Planum is the site of either local mantle downwelling [*Bindschadler et al.*, 1990; *Bindschadler and Parmentier*, 1990], or local mantle upwelling [*Grimm and Phillips*, 1990, 1991], producing crustal contraction. A third model, [*Crumpler et al.*, 1986; *Head*, 1990] proposes that Ishtar Terra is the locus of regional compression, with crust converging on, and subducting beneath, Lakshmi Planum.

Bindschadler and Parmentier [1990] and *Bindschadler et al.* [1990, 1992] propose that deformation around Ishtar Terra results from crustal thickening and contraction above a cylindrical mantle downwelling. According to these workers, vertical normal stresses from downward flow, and shear coupling of horizontal mantle flow with the base of the crust, cause flow and thickening in the lower crust and resultant surface uplift and contractional deformation. Using Andersonian criteria, *Bindschadler et al.* [1990] predicted a relative deformation sequence with increasing crustal thickness as follows: (1) radial thrusts above the downflow and strike-slip faults toward the periphery; (2) radial and concentric thrust faults, with strike-slip faults toward the periphery; (3) outward migration of radial thrusting and strike-slip motion at the center of the uplift; and (4) at steady-state, radial normal faulting and strike-slip faults. Contraction is inferred to young outward from the periphery of the belt.

In contrast, *Grimm and Phillips* [1990, 1991] propose that Lakshmi Planum records crustal thickening above an upwelling mantle plume, and that crustal thickening and mountain belt deformation result from downward return flow of the plume. Structures predicted using Andersonian criteria are similar to those postulated by *Bindschadler et al.* [1990], including initial radial thrust faults with peripheral strike-slip faults, changing to concentric thrust faults with peripheral radial thrust faults, and ultimately to radial normal faults and peripheral strike-slip faults with time and increasing crustal thickness. Contraction is inferred to young inward from the periphery of the belt.

Both models predict contractional structures oriented both radially and concentrically with respect to Lakshmi Planum, and abundant peripheral strike-slip faults at various stages of uplift. None of the structures on Maxwell are radially oriented around Lakshmi; rather, orientations of each of the structural suites are uniform across Lakshmi Planum and cannot easily be interpreted as concentric. Predictions as to the younging direction of structures on Maxwell cannot be tested because temporal relations parallel to strike cannot be determined. Both of these models therefore predict structures that are not observed, and fail to predict observed structural relations [see also *Phillips and Hansen*, 1994; *Hansen and Phillips*, 1993], and neither model discusses how stresses within the mantle are transferred to the crust. Both models suggest that mountain belts result from thickened crust. If this were true, the highest elevations, underlain by the thickest crust, would be the loci of gravitational collapse; yet this is not observed. Also, recent gravity data [*Sjogren*, 1993] suggest that western Ishtar Terra may have a larger component of crustal compensation than previously thought, and therefore geodynamic models may not need to infer deep-mantle flow mechanisms. It is possible that the gravity data used for both of these models may result from both long- and short-wavelength compensation mechanisms.

Although both studies are modeled at scales far greater than that of individual Ishtar deformed belts, and make few unique

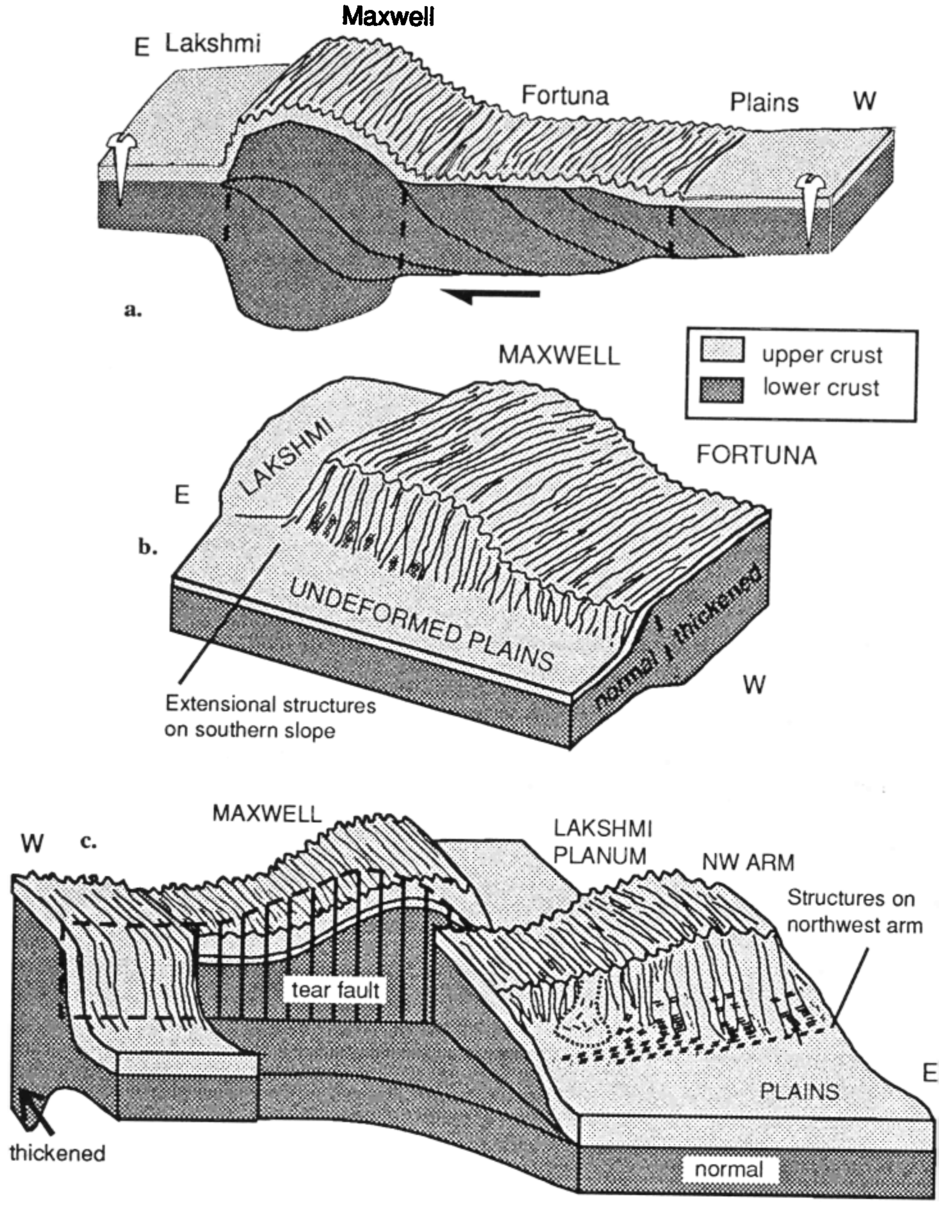

Figure 7. (a) Schematic cross section from Lakshmi Planum east toward Fortuna Tessera, showing proposed changes in mantle residuum thickness that support Maxwell Montes. (b) Schematic block diagram indicating the relationship between mantle residuum thickness and the location of extensional structures. Extension occurs only in areas of steep topography that mark the transition from crust overlying thickened residuum to crust overlying normal residuum. Figure has same spatial orientation as Figure 7a. (c) Schematic block diagram looking south from the NW arm to the main body of Maxwell, illustrating the tear fault origin proposed for the 0°E lineament. A section of crust/mantle is shown removed for illustrative purposes. Note that the tear fault does not everywhere intersect the surface; in fact it may not intersect the surface at all.

predictions as to the nature of crustal deformation, they may, with modifications, provide insights into possible processes driving crustal deformation. The presence of a variety of volcanic constructs on Venus have led many authors to propose that Venus looses much of its heat through mantle plumes rising to the surface [see review in *Phillips and Hansen*, 1994]. It is possible that plume activity at some scale may be responsible for some of the features of Ishtar Terra, and we explore this possibility more fully below (see Proposed Tectonic Model for Maxwell Montes).

A third model for the tectonic evolution of Ishtar Terra, similar to plate tectonic models for Earth, is regional compression [e.g., *Crumpler et al.*, 1986; *Head*, 1990; *Roberts and Head*, 1990]. In this model, based on deformation analyses of the surface using Venera images, the Ishtar deformed belts result from crustal thickening as a result of underthrusting of lithosphere under Lakshmi Planum. Such a plate convergence model would predict (1) variations in strain intensity, with high strain at the plate boundary, and lower strain away from it; (2) major structures parallel to plate margins, with nonorthogonal convergence accommodated as margin-parallel displacements; (3) gradual lateral termination of intense deformation, with possible transition to different structures (e.g., termination of terrestrial orogenic belts at bounding strike-slip faults); and (4) extensional collapse of the deformation belt during later stages of convergence. The kinematic patterns predicted by this model are not observed in Maxwell Montes, or regionally throughout Ishtar Terra [*Phillips and Hansen*, 1994]. We reject a regional compression model because predicted surface structures are not observed, and crustal thickening is inferred to be solely due to crustal deformation, yet the observed small-wavelength and small amplitude structures, interpreted as folds and thrusts, cannot account for the topography of Maxwell . In fact, crustal thickening on the order of only several kilometers is predicted [e.g., *Vorder Bruegge*, 1994].

Tectonic Models for Maxwell Montes

Pre-Magellan models for the formation of Maxwell Montes, based on a thorough analysis of Venera and Arecibo data [*Vorder Bruegge and Head*, 1989; *Vorder Bruegge et al.*, 1990], propound that Maxwell Montes comprises ten distinct crustal domains, forming an original, linear, terrestrial-style mountain belt, telescoped along nine right-lateral strike-slip faults (with up to 125 km displacement/fault). The telescoped package is proposed to lie between two bounding shear zones, a northeast-striking, right-lateral zone at the northern boundary, and an east-striking, left-lateral zone at the southern boundary, along which Maxwell Montes was rotated and translated into its present configuration. This model hinges on the identification of nine north-northwest-trending strike-slip faults and two crustal-scale shear zones that are not documented with Magellan data [*Kaula et al.*, 1992; *R. W. Vorder Bruegge, personal communication*, 1993; this study]. However, even with relatively low-resolution data, certain structural features were identified [*Vorder Bruegge et al.*, 1990]: (1) the sigmoidal nature of the penetrative lineaments; (2) grabens spatially restricted to northern and southern slopes; and (3) a lack of extensional features on central Maxwell, indicating stability of the belt .

Using Magellan data, *Suppe and Connors* [1992] proposed that deformation of the steep western slope of Maxwell Montes resulted from east-directed underthrusting of Lakshmi Planum beneath Maxwell Montes, analogous to the toe of a critical-taper wedge as proposed for terrestrial fold and thrust deformation. This model addresses only deformation on the western slope of Maxwell and does not explain other deformation fabrics or structural features. Because the structures present along the western slope are not limited to this region, but extend to the rest of Maxwell, we believe that any model must address formation of the entire range and its structures, not simply a small part thereof.

Proposed Tectonic Model for Maxwell Montes

Our proposed model for the tectonic evolution of Maxwell Montes seeks to explain the following observations and interpretations: (1) broadly distributed surface strain, with little change in intensity over hundreds of kilometers perpendicular to strike or elevation changes of several kilometers; (2) inability of short-wavelength/small amplitude structures to support topography; (3) apparent stability of crust within the mountain belt, particularly at the highest elevations; (4) abrupt termination of deformation, corresponding to steep topographic gradient; and (5) that evidence for extension is limited to areas of steep topographic slope.

The apparent short wavelengths and small amplitudes of structures on Maxwell Montes, coupled with their broad distribution, indicate that they represent little more than surface deformation of a thin layer, analogous to contractional and shear structures in flowing lava that develop as the cool surface of the flow is decoupled from and dragged along with the flowing lava underneath [*Borgia et al.*, 1983]. If this analogy is correct, it implies that processes occurring in the region below the thin surface layer are responsible for the surface deformation of Maxwell Montes. Also, as we have noted, the small amplitudes of Maxwell deformation structures are unable to account for the high topography, yet Maxwell is apparently stable, with no evidence of extensional collapse even at the highest elevations. This also strongly implies that the mountain belt is being supported from below, by processes operating at deeper levels than the thin upper crust. Finally, the Maxwell structures preserve no apparent strain gradient across the deformed belt; structural spacing remains unchanged despite large topographic changes.

We follow the model of *Phillips and Hansen* [1994; *Hansen and Phillips*, 1993], that deformation in the mountain belts surrounding Lakshmi Planum are surface manifestations of deformation processes occurring at depth in the crust and mantle (deformation-from-below model). In this model, the strong, upper crust is separated from a strong lower crust by a weak zone (a "jelly sandwich" analogy) [e.g., *Zuber*, 1987; *Banerdt and Golombek*, 1988] (Figure 7). The upper crust may be broadly decoupled from the lower crust [*Basilevsky et al.*, 1986; *Phillips*, 1986, 1990] by a weak layer that acts as both a decollement surface, allowing the upper crust to deform independently, and as a stress conduit, transmitting lower crustal and mantle stresses to the upper crust. The upper crust therefore deforms independently of the lower crust, but in response to stresses imposed by mantle strain episodes. Large-scale deformation in the lower crust and mantle will thus be manifested as "cover" deformation in the upper crust (Figure 7).

Upper-mantle melt residuum ponds at depth beneath Ishtar, drawn downward and inward as a result of mantle downwelling [*Phillips and Hansen* , 1994; *Hansen and Phillips*, 1993]. Maxwell Montes is underlain by imbricated lower crust, stacked up as a result of the ponding residuum; thickened lower crust supports the mountain-belt-scale topography (Figure 7). Upper crustal "cover" deforms passively in response to lower-crustal translation, imbrication and thickening. Structurally imbricated lower crust would have steep boundaries at the front and sides (western slope and northern and southern slopes of Maxwell, respectively), and shallow boundaries behind the imbricated package (eastern slope of Maxwell) [*Dahlstrom*, 1970; *Butler*, 1982; *Boyer and Elliot*, 1982; *Mitra*, 1986]. At the center of the uplifted area, structures are supported and thus stable (Figure 7). At the periphery, sharp boundaries exist between upper crust that overlies normal lower crust and mantle and upper crust that overlies thickened lower crust. Upper crust overlying thickened lower crust is stretched to accommodate the increased surface area created by the thickening (much like a table cloth is stretched out over a table). At the boundaries between thickened and unthickened areas, contractional structures will end abruptly, and extensional structures accommodate the increased surface area (Figure 7). In this model then, the lower crust thickens and supports the mountian-belt scale topography, whereas a pond, or kneel of residuum supports the long-wavelength (2,000 km) welt of Ishtar Terra. This keel of mantle residuum would be similar to mantle keels beneath continents on Earth [*Jordan*, 1975, 1981]. The thickened upper-mantle residuum (and possibly mantle downwelling) is responsible for the large apparent depth of compensation at the wavelength of Ishtar Terra. The high elevation of Maxwell is supported by variably thickened lower crust, and detailed topography is associated with folded, modestly thickened crust [*Phillips and Hansen*, 1994; *Hansen and Phillips*, 1993].

The 0°E lineament between central Maxwell and the northwest arm marks changes in slope facing direction, and the spatial limit of localized gravity sliding. It may be accommodated within the above described "deformation-from-below" model as a surface manifestation of a lateral ramp or tear fault, bounding the imbricated lower crustal package. Terrestrial fold and thrust belts are not continuous along strike; differential displacement on different parts of the system are accommodated by tear faults or transform faults that segment the belt (Figure 7). Thrust systems may terminate laterally at these structures, much like the Lewis thrust of the northern Rocky Mountains, or the Pine Mountain thrust of the Appalachian Mountains [*Dahlstrom*, 1970; *Boyer and Elliot*, 1982; *Butler*, 1982; *Mitra*, 1986]. We propose that during lower crustal imbrication differential displacement on the overthrust sheet was accommodated by a tear fault or lateral ramp beneath what is now the discontinuity between central Maxwell and the northwest arm (Figure 7c). This fault was activated late in the deformation history, after similar structural suites had developed ubiquitously across Maxwell. Activation of the tear fault at depth may have mechanically separated the residuum beneath the northwest arm from that beneath central Maxwell, with failure triggering gravity sliding on the arm. Movement on the fault may also have caused the arm to be translated westward, resulting in the apparent offset of the arm from central Maxwell.

Recently acquired gravity data, and newly derived flow laws for Venus may have implications for the proposed model. New deformation experiments for materials scaled to the crust of Venus [*Mackwell et al.*, 1994] indicate that the depth-averaged strength of the crust may be more similar to that of the mantle than previously thought. Thus the strong-weak-strong profile may be less distinct than indicated by previous experiments [*Zuber*, 1994]. Preliminary evaluation of the relationship between tectonic length scales and a strong layer thickness [*Neumann and Zuber*, 1994] indicates that multiple deformation may still occur when brittle-ductile transitions occur in both the crust and the upper mantle. Also, even with a much stronger crust, contractional morphologies on Venus may be explained by horizontal shortening of a laterally heterogeneous lithosphere [*Zuber et al.*, 1994]. Strain rate is also important, and development of the observed short-wavelength structures on Maxwell with a stronger crust as proposed by new flow laws, requires low strain rates. Alternately, the structures may have formed at a time when the crust had not yet attained its present proposed strength, thus implying a relative age for Maxwell deformation. It must be remembered that the diabase flow laws used in estimating crustal strength are highly sensitive to grain size and feldspar content, changes in which may produce significantly different strengths [*Zuber*, 1994].

We therefore conclude that passive deformation of upper-crustal material over an imbricating lower crustal layer explains the broad strain distribution and the uniformity of strain over hundreds of kilometers perpendicular to strike and across elevation changes of several kilometers. Such passive deformation results in short-wavelength structures that are incompatible with high topography, implying support of the upper crust by underlying thickened lower crust and thickened mantle residuum. Support from below also explains the lack of extensional collapse of the surface features, the abrupt termination of deformation at slope boundaries, and the distribution of extensional structures limited to these boundaries. Tear faulting during lower crustal imbrication may have triggered gravity sliding on the northwest arm, explaining the discontinuity between the northwest arm and central Maxwell.

Conclusions

The following conclusions can be drawn from this study: (1) central Maxwell and the northwest arm record similar deformation histories, with the northwest arm recording a late episode of gravity sliding; (2) the aspect ratio, abrupt along-strike termination of deformation at the base of the steep northern and southern slopes, and the broadly distributed strain on and around Maxwell Montes make it unlike terrestrial deformation belts; (3) the modest shortening indicated by short-wavelength structures on Maxwell is unable to account for the great elevation of the belt; (4) Maxwell Montes may be underlain by a "block" of anomalously thickened lower crust that supports mountain-belt-scale topography and controls the spatial distribution of deformation; and (5) failure along a possible lower crustal tear fault bounding the anomalously thickened lower crust may have resulted in gravity sliding structures on the northwest arm.

Acknowledgments. This research was supported by NASA operating grant NAGW-2915 awarded to V.L.H. We thank John Goodge for his suggestions and comments, and Bruce Banerdt and Bob Grimm for their reviews. Warm thanks also to Dianne Hess Goldbach for her patience, support and marvelous humour.

References

Banerdt, W. B., and C. G. Sammis, Small-scale fracture patterns on the volcanic plains of Venus, *J. Geophys. Res.*, *97*, 16,149-16,166, 1992.

Banerdt, W. B. and M. P. Golombek, Deformation models of rifting and folding on Venus, *J. Geophys. Res.*, *93*, 4759-4772, 1988.

Basilevsky, A. T., Structure of central and eastern areas of Ishtar Terra and some problems of Venusian tectonics, *Geotectonics*, *20*, 282-288, 1986.

Basilevsky, A. T., A. A. Pronin, L. B. Ronca, V. P. Kryuchkov, A. L. Sukhanov, and M. S. Markov, Styles of tectonic deformations on Venus: analysis of Venera 15 and 16 data, *Proc. Lunar Planet. Sci. Conf. 16th, Part 2, J. Geophys. Res.*, *91*, suppl., D399-D411, 1986.

Berthé, D., P. Choukroune, and P. Jegouzo, Orthogneiss, mylonite and non-coaxial deformation of granites: the example of the South American shear zone, *J. Struct. Geol.*, *1*, 31-42, 1979.

Bindschadler, D. L., G. Schubert, and W. M. Kaula, Coldspots and hotspots: global tectonics and mantle dynamics of Venus, *J. Geophys. Res.*, *97*, 13495-13532, 1992.

Bindschadler, D. L., and J. W. Head, Tessera terrain, Venus: characterization and models for origin and evolution, *J. Geophys. Res.*, 96, 5889-5907, 1991.

Bindschadler, D. L., and E. M. Parmentier, Mantle flow tectonics: the influence of a ductile lower crust and implications for the formation of topographic uplands on Venus, *J. Geophys. Res.*, *95*, 21,329-21,344, 1990.

Bindschadler, D. L., G. Schubert and W. M. Kaula, Mantle flow tectonics and the origin of Ishtar terra, Venus, *Geophys. Res. Lett.*, *17*, 1345-1348, 1990.

Bindschadler, D. L., G. Schubert, and W. M. Kaula, Coldspots and hotspots: global tectonics and mantle dynamics of Venus, *J. Geophys. Res.*, *97*, 13495-13532, 1992.

Borgia, A., S. Linneman, D. Spencer, L. D. Morales and J. B. Andre, Dynamics of lava flow fronts, Arenal volcano, Costa Rica, *J. Volcanol. Geotherm. Res.*, *19*, 303-329, 1983.

Boyer, S. E., and D. Elliot, Thrust systems, *AAPG. Bull.*, *66*, 1196-1230, 1982.

Butler, R. W. H., The terminology of structures in thrust belts, *J. Struct. Geol.*, *4*, 239-245, 1982.

Campbell, D. B., J. W. Head, and A. A. Hine, Venus: identification of banded terrain in the mountains of Ishtar Terra, *Science, 221*, 644-647, 1983.

Crumpler, L. S., J. W. Head, and D. B. Campbell, Orogenic belts on Venus, *Geology*, *14*, 1031-1034, 1986.

Dahlstrom, C. D. A., Structural geology in the eastern margin of the Canadian Rocky Mountains, *Bull. Can. Pet. Geol.*, *18*, 332-406, 1970.

Engelder, T., and P. Geiser, On the use of regional joint sets as trajectories of paleostress fields during the development of the Appalachian plateau, New York, *J. Geophys. Res.*, *85*, 6319-6341, 1980.

Farr, T. G., Radar interaction with geologic surfaces, in Guide to Magellan Image Interpretation, edited by J. P Ford et al., *JPL Publ* , *93-24*, 45-56, 1993.

Ford, J. P., R. G. Blom, J. A. Crisp, C. Elachi, T. G. Farr, R. S. Saunders, E. E. Theilig, S. D. Wall and S. B. Yewell, 126 pp., *Spacebourne Radar Observations - A Guide for Magellan Radar-Image Analysis*, Jet Propulsion Laboratory, Pasadena, Calif., 1989.

Ford, J. P., J. J. Plaut, C. M. Weitz, T. G. Farr, D. A. Senske, E. R. Stofan, G. Michaels and T. J. Parker, (Eds.), Guide to Magellan Image Interpretation, *JPL Publ.*, *93-24*, 1993.

Ford, P. G., and G. H. Pettengill, Venus topography and kilometer-scale slopes, *J. Geophys. Res.*, *97*, 13103-13114, 1992.

Grimm, R. E., and R. J. Phillips, Tectonics of Lakshmi Planum, Venus: tests for Magellan, *Geophys. Res. Lett.*, *17*, 1349-1352, 1990.

Grimm, R. E., and R. J. Phillips, Gravity anomalies, compensation mechanisms, and the geodynamics of western Ishtar Terra, Venus, *J. Geophys. Res.*, *96*, 8305-8324, 1991.

Hansen, V. L., and R. J. Phillips, Ishtar deformed belts: evidence for deformation from below? (abstract) *Lunar Planet. Sci.*, 24, 603-604, 1993.

Head, J. W., Formation of mountain belts on Venus: evidence for large-scale convergence, underthrusting, and crustal imbrication in Freyja Montes, Ishtar Terra, *Geology*, *18*, 99-102, 1990.

Jordan, T. H., The continental tectosphere, *Rev. Geophys.*, *13*, 1-12, 1975.

Jordan, T. H., Continents as a chemical boundary layer, *Phil. Trans. R. Soc. London, A*, *301*, 359-373, 1981.

Kaula, W. M., D. L. Bindschadler, R. E. Grimm, V. L. Hansen, K. M. Roberts, and S. S. Smrekar, Styles of deformation in Ishtar Terra and their implications, *J. Geophys. Res.*, *97*, 16085-16120, 1992.

Kiefer, W. S., and B. H. Hager, The role of mantle convection on the formation of highland regions on Venus (abstract), *Lunar Planet. Sci.*, *20*, 520-521, 1989.

Lenardic, A., W. M. Kaula, and D. L. Bindschadler, The tectonic evolution of western Ishtar Terra, Venus, *Geophys. Res. Lett.*, *18*, 2209-2212, 1991.

Mackwell, S. J., M. E. Zimmerman, D. L. Kohlstedt, and D. S. Scherber, Dry deformation of diabase: implications for tectonics of Venus, *Lunar Planet. Sci.*, *25*, 817-818, 1994.

Mitra, S., Duplex structures and imbricate thrust systems: geometry, structural position and hydrocarbon potential, *AAPG Bull.*, *70*, 1087-1112, 1986.

Neumann, G. A., and M. T. Zuber, Patterns of brittle deformation under extension on Venus (abstract), *Lunar Planet. Sci.*, *25*, 993-994, 1994.

Pettengill, G. H., P. G. Ford, W. T. K. Johnson, R. K. Raney and L. A. Soderblom, Magellan: radar performance and data products, *Science*, *252*, 260-265, 1991.

Phillips, R. J., A mechanism for tectonic deformation on Venus, *Geophys. Res. Lett.*, *13*, 1141-1144, 1986.

Phillips, R. J., Convection-driven tectonics on Venus, *J. Geophys. Res.*, *95*, 1301-1316, 1990.

Phillips, R. J., and V. L. Hansen, Tectonic and magmatic evolution of Venus, *Ann. Rev. Earth Planet. Sci.*, *22*, 597-654, 1994.

Pollard, D. D., and A. Aydin, Progress in understanding jointing over the past century, *Geol. Soc. Am. Bull.*, *100*, 1181-1204, 1988.

Pronin, A. A., The structure of Lakshmi Planum, and indication of horizontal and asthenospheric flow on Venus, *Geotectonics, 20*, 271-281, 1986.

Ramsay, J. G., and M. I. Huber, The Techniques of Modern Structural Geology, 307 pp., Academic, San Diego, Calif., 1983.

Roberts, K. M., and J. W. Head, Western Ishtar Terra and Lakshmi Planum, Venus: models of formation and evolution, *Geophys. Res. Lett.*, *17*, 1341-1344, 1990.

Saunders, R. S. and G. H. Pettengill, Magellan: Mission summary, *Science*, *252*, 247-249, 1991.

Saunders, R. S., et al., Magellan mission summary, *J. Geophys. Res.*, *97*, 13067-13090, 1992.

Shreve, R. L., The Blackhawk landslide, *Spec. Pap. Geol. Soc. Am.*, *108*, 47 pp., 1968.

Sjogren, W. L., Results from newly aquired Venus gravity data, *Eos Trans. AGU*, *74 (43)*, Fall Meeting suppl., 374, 1993.

Smrekar, S. E., and S. C. Solomon, Gravitational spreading of high terrain in Ishtar Terra, Venus, *J. Geophys. Res.*, *97*, 16,120-16,148, 1992.

Solomon, S. C., J. W. Head, W. M. Kaula, D. McKenzie, B. Parsons, R. J. Phillips, G. Schubert, and M. Talwani, Venus tectonics: initial analysis from Magellan, *Science*, *252*, 297-312, 1991.

Solomon, S. C., et al., Venus tectonics: an overview of Magellan observations, *J. Geophys. Res.*, *97*, 13,199-13,255, 1992.

Stofan, E. R., D. A. Senske and T. J. Parker, Tectonic features in Magellan data, in Guide to Magellan Image Interpretation, edited by J. P. Ford et al., *JPL Publ.* , *93-24*, 93-108, 1993.

Suppe, J., and C. Connors, Critical taper wedge mechanics of fold-thrust-belts on Venus: Initial results from Magellan, *J. Geophys. Res.*, *97*, 13,545-13,562, 1992.

Tyler, G. L., R. A. Simpson, M. J. Maurer and E. Holmann, Scattering properties of the Venusian surface: preliminary results from Magellan, *J. Geophys. Res.*, *97*, 13,115-13,140, 1992.

Varnes, D. J., Landslide types and processes, Landslides and Engineering Practice, *Spec. Rep. 29*, pp. 20-47, Natl. Acad. of Sci., Natl. Res Counc. Highway Res. Board, Washington D. C., 1958.

Vorder-Bruegge, R. W., Variation in compressional structures across Maxwell Montes: evidence for a sequence of events in a venusian orogeny (abstract), *Lunar Planet. Sci..*, *25*, 1449-1450, 1994.

Vorder-Bruegge, R. W., and J. W. Head, Fortuna Tessera, Venus: evidence of horizontal convergence and crustal thickening, *Geophys. Res. Lett.*, *16*, 699-702, 1989.

Vorder-Bruegge, R. W., J. W. Head and D. B. Campbell, Orogeny and large-scale strike-slip faulting on Venus: tectonic evolution of Maxwell Montes, *J. Geophys. Res.*, *95*, 8357-8381, 1990.

Zuber, M. T., Constraints on the lithospheric structure of Venus from mechanical models and tectonic surface features, *J. Geophys. Res* , *92*, 541-551, 1987.

Zuber, M. T., Rheology, tectonics, and the structure of the Venus lithosphere (abstract), *Lunar Planet. Sci.*, *25*, 1575-1576, 1994.

Zuber, M. T., E. M. Parmentier, and G. A. Neumann, Formation of fold and thrust belts on Venus due to horizontal shortening of a laterally heterogeneous lithosphere, *Lunar Planet. Sci.*, *25*, 1577-1578, 1994.

V. L. Hansen and M. Keep, Department of Geological Sciences, Southern Methodist University, Dallas, TX 75275. (email: myra@saturn.isem.smu.edu)

(Received October 4, 1993; revised June 4, 1994; accepted September 30, 1994.)